Probing Unfolded Acoustic Phonons with X Rays

M. Trigo,[1,*] Y. M. Sheu,[1] D. A. Arms,[2] J. Chen,[1] S. Ghimire,[1] R. S. Goldman,[3] E. Landahl,[2,†] R. Merlin,[1] E. Peterson,[1] M. Reason,[3] and D. A. Reis[1]

[1]*Department of Physics, University of Michigan, Ann Arbor, Michigan 48109, USA*
[2]*Advanced Photon Source, Argonne, Illinois 60439, USA*
[3]*Department of Materials Science and Engineering, University of Michigan, Ann Arbor, Michigan 48109, USA*

(Received 6 May 2008; published 11 July 2008)

Ultrafast laser excitation of an InGaAs/InAlAs superlattice (SL) creates coherent folded acoustic phonons that subsequently leak into the bulk (InP) substrate. Upon transmission, the phonons become ''unfolded'' into bulk modes and acquire a wave vector much larger than that of the light. We show that time-resolved x-ray diffraction is sensitive to this large-wave vector excitation in the substrate. Comparison with dynamical diffraction simulations of propagating strain supports our interpretation.

DOI: 10.1103/PhysRevLett.101.025505 PACS numbers: 63.22.−m, 78.47.−p

High-frequency acoustic phonons with large wave vectors and short mean free paths play a fundamental role in heat transport and energy relaxation in solids [1]. In particular, in insulators these modes are the dominant carriers of heat. The combination of their short wavelengths and relatively low energies make them a unique probe of interfaces and nanoscale structures [2]. Thus, there is great interest in the generation and detection of coherent acoustic modes with such characteristics. Ultrafast laser pulses, together with the branch folding that occurs in a superlattice (SL), provide a convenient method to coherently excite these phonons [3]. However, direct detection of high-wave-vector modes cannot be attained by standard light scattering techniques that only probe wave vectors near the Brillouin zone center. In this Letter, we report the first direct observation of the unfolded modes via wave vector resolved time-domain x-ray diffraction.

Time-resolved x-ray diffraction (TRXD) is a sensitive probe of the ultrafast atomic motion associated with coherent phonons [4]. Recently, TRXD has been utilized to study coherent zone-center folded modes within a superlattice using femtosecond resolution from a laser-plasma source [5] and a picosecond resolution from a third generation synchrotron [6]. In the latter case, a streak camera was used to achieve few picosecond resolution from the ~100 ps pulse duration typical of a synchrotron. In this experiment, we use synchrotron-based TRXD to detect propagating bulk modes with high-wave-vector that originated as zone-folded modes in a SL. While 100 ps resolution is not fine enough to measure the real-time atomic displacements associated with THz phonons, the presence of large-wave vector modes (such as the zone-unfolded modes) nonetheless manifests itself as high-momentum sidebands of an x-ray diffraction peak. Here the time-resolution serves as a gate to sample the modes as they propagate deep into the bulk.

Experiments were performed at room temperature on a 60-period SL with layers composed of $Ga_{0.47}In_{0.53}As$ and $Al_{0.48}In_{0.52}As$ of thicknesses 12.3 and 4.7 nm, respectively, grown by molecular beam epitaxy on an (001) InP substrate. Coherent longitudinal folded phonons were generated using ~50 fs pulses from an amplified Ti:sapphire laser (central wavelength of 800 nm) at the rate of 5 kHz. The 200 μJ laser pulses were focused near collinearly with monochromatic, collimated x-ray pulses to a $\sim 2 \times 6$ mm^2 spot on the sample yielding an incident fluence of ~2 mJ/cm^2. Because the laser spot-size is much larger than the ~250 nm absorption length, only coherent longitudinal modes are excited along the [001] direction. The hard x-ray probe pulses from the sector-7 undulator at the Advanced Photon Source were monochromatized with a double diamond (111) monochromator to an energy of 10.3 keV, below the absorption edge of the gallium. Active feedback control of the laser cavity length was used to synchronize the laser and x-ray repetition rates [7]. A phase shifter was used to achieve time delays with a resolution of 19 ps, finer than the x-ray pulse duration of ~100 ps. Using a grazing-incidence rhodium-coated curved mirror to focus the x-ray beam in the horizontal direction suppresses the x-ray harmonics and increases the x-ray flux with only a minor reduction in the angular resolution. The scattering takes place in the vertical plane, perpendicular to the x-ray polarization. The sample was mounted on a six-circle Huber diffractometer that allows precise control of the sample orientation and the detector position. The diffracted signal was recorded with a fast avalanche photodiode able to resolve individual x-ray pulses from the synchrotron. Two subsequent x-ray pulses from the same electron bunch in the storage ring were isolated by electronically gating the diffracted signal, such that the intensity after, I_{on}, and 3.6 μm before the laser, I_{off}, could be recorded [8]. The folded phonon period of 3.85 ps was obtained by transient reflectivity measurements with pulses from a 250 kHz Ti:sapphire laser in a standard pump-probe setup.

Figure 1 shows static results as well as TRXD data that will be discussed later. The static diffraction pattern for 10.3 keV x-rays near the (004) symmetric Bragg reflection of the InP substrate (solid line in Fig. 1, top panel) shows three SL sidebands, labeled (±1) and (−2), as well as the

Bragg peak from the average lattice planes of the constituents of the SL, labeled (0). In terms of the larger unit cell of the SL, these peaks correspond to x-ray diffraction from $(00L)$ planes of the SL, with $L = 114$–117. The depth of the x-ray probe is limited by absorption to $\sim 6\ \mu$m, which is substantially longer than the SL thickness. Consequently, the (004) peak of the substrate is also observed (labeled InP). This peak appears at an angle lower than that of (0), indicating that the lattice parameter of InP is larger than that of the SL. The InP x-ray diffraction peak from the back surface of the 0.35 mm-thick substrate is limited by the experimental resolution of ~ 3 mdeg, while the front side reflection shown in Fig. 1 is broadened, with an angular width of 21 mdeg, likely due to strain. Figure 1 also shows the calculated dispersion relation [9] of the longitudinal acoustic waves in the SL in the extended-zone scheme (bottom panel, solid curve). We have shifted the origin of the SL dispersion relation to align with the (0) peak and we have adjusted the period D slightly to match the position of the (± 1) sidebands in the experiment. The dashed line in the lower panel is the longitudinal acoustic dispersion relation in the InP substrate, i.e. $\omega = vq$, where v is the longitudinal speed of sound in InP.

The SL phonons satisfy the bulk acoustic dispersion relation upon transmission into the substrate. Thus, by energy conservation, the folded phonons acquire a wave vector $q^* = 2\pi/D^*$, where $D^* = v/v_{\mathrm{SL}}D$, is the wavelength of the phonon in the substrate and v_{SL} is the average speed of sound in the SL. This wave vector transfer corresponds approximately to the angular separation between the (0) and the (± 1) peaks. Note that the Brillouin zone of the substrate is centered at the (004) Bragg peak of the InP instead of the (0) peak of the SL, so that the wave vector transfer is referenced to the InP peak. Hence, the folded phonons that leak into the substrate are expected to produce features at angular positions $\theta = \theta_{\mathrm{InP}} \pm q^*/G \cot\theta_{\mathrm{InP}}$, where G is the (004) reciprocal lattice vector of InP and θ is the Bragg angle.

Figure 2 shows time-resolved data on the lower side of the (-1) sideband. The false-color scale represents the $I_{\mathrm{on}}/I_{\mathrm{off}}$ ratio, that is, the diffracted intensity in the laser-on gate normalized to the intensity when the laser arrives after the x-ray pulse. Absorption of the laser pulse produces a lattice expansion that shifts the diffraction curve towards lower angles [8]. The prominent $t = 0$ feature at $\theta = 24.08°$ is due to this shift of the (-1) sideband. The laser-induced stress in the SL generates acoustic strain that leaks subsequently into the substrate. This acoustic pulse comprises high-frequency longitudinal modes in the folded branches that propagate into the substrate at the speed of sound [10]. This high-frequency, short wavelength component of the strain appears in Fig. 2 at an angle $\theta = 24.04°$ corresponding to the wave vector of the SL phonons un-

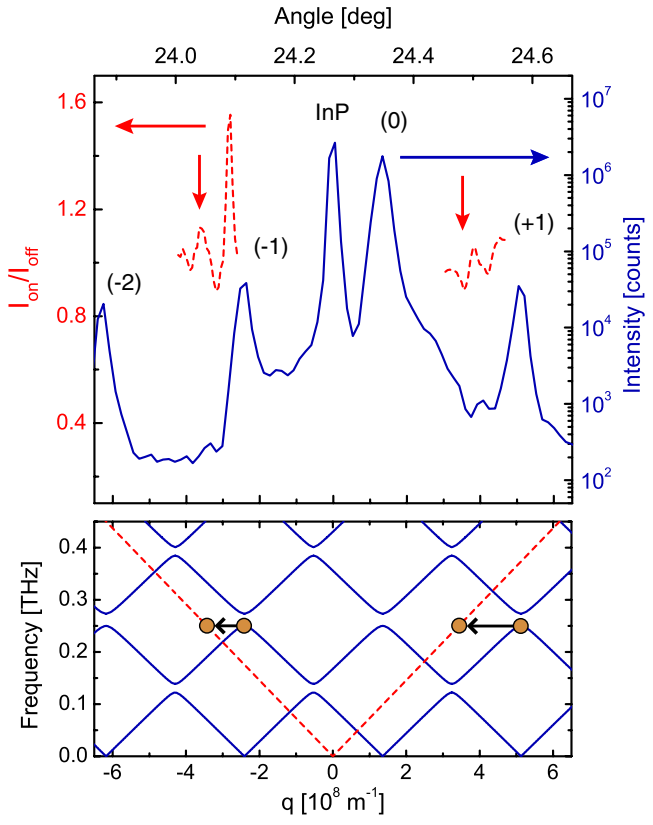

FIG. 1 (color online). (Top panel) Static x-ray diffraction from a 60-period superlattice with layers of $Ga_{0.47}In_{0.53}As$ and $Al_{0.48}In_{0.52}As$ with thicknesses 12.3 and 4.7 nm, respectively, on an (001) InP substrate (solid line). The dashed lines are slices of $I_{\mathrm{on}}/I_{\mathrm{off}}$ at $t = 0.2$ ns for wave vectors below the (-1) and the $(+1)$ sidebands. (lower panel) Dispersion relation for the acoustic waves in the SL (solid curve). Dispersion relation for the acoustic waves in the substrate (dashed line).

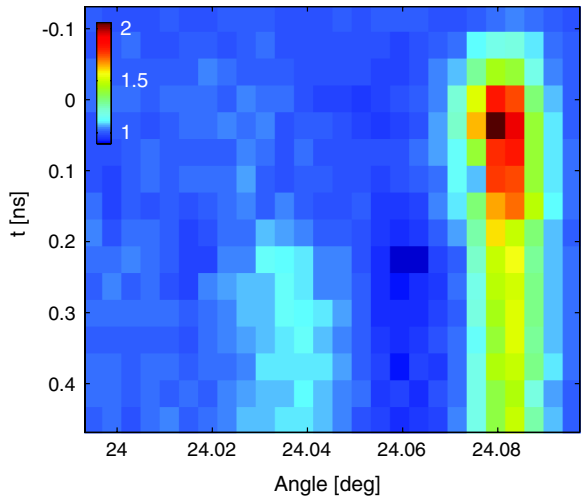

FIG. 2 (color online). Ratio $I_{\mathrm{on}}/I_{\mathrm{off}}$ as a function of time delay at the expected angular position for the folded phonons below the (-1) sideband. The feature at 24.08° is the shift of the (-1) peak due to thermal expansion induced by the laser pulse. At $t = 0.2$ ns, the signature from unfolded phonons in the substrate appears at $\theta = 24.04°$, which corresponds to a wave vector transfer $q^* = 2\pi/D^*$.

folded into the substrate. This feature appears delayed from $t = 0$ by the transit time through the SL, ~0.2 ns.

To facilitate the interpretation of these results and to compare with the acoustic dispersion relation, we converted the measured angles to the corresponding reciprocal-space wave vector, q, referenced relative to the Bragg peak of the InP. Figure 1 presents the data in the wave vector picture. Superimposed on the static diffraction pattern we show data at $t = 0.2$ ns (dashed line) of the time-resolved scan presented in Fig. 2, along with a similar scan near the $(+1)$ sideband. To correct for small systematic errors in the goniometer position, we shifted these curves horizontally to align the I_{off} trace with common features in the static data. The wave vectors of the first zone-folded phonons in the extended Brillouin-zone are indicated with filled circles on the dispersion relation in the lower panel. These are corroborated by independent optical pump-probe measurements of the phonon frequency. The vertical arrows in the top panel indicate the wave vector at which the unfolded phonons are expected. The arrows are in good agreement with the features from TRXD, however, the $(+1)$ trace does not match the expected wave vector as well as the (-1). This could be due to a small systematic error in the goniometer positioning or a difference in the calculated and actual phonon dispersion.

To corroborate our assignments, we calculated the time-dependent diffraction patterns by solving the Takagi-Taupin equations [11,12] from the theory of dynamical diffraction of x rays [13], modified to incorporate acoustic strain [14]. To simplify the calculations, we took the initial strain to be Gaussian modulated and localized in the SL (Fig. 3). This simplifies the boundary conditions while preserving the key features related to the folded phonons. The atomic displacement, $u(z)$, evolves according to [3]

$$\rho(z)\frac{\partial^2 u(z,t)}{\partial t^2} = \frac{\partial}{\partial z}\left[C(z)\frac{\partial u(z,t)}{\partial z}\right], \quad (1)$$

where $C(z)$ is the elastic stiffness coefficient and $\rho(z)$ is the density of the constituents. The strain $\eta = \partial u/\partial z$, associated with the longitudinal displacement, u, is along the growth direction, z. We set the peak of the initial strain to be $\sim 3 \times 10^{-4}$, which is consistent with our laser fluence [5]. The boundary condition $\eta(0, t) = 0$ at the SL-air surface together with a smooth initial condition avoids sharp edges that introduce high-frequency artifacts in the numerical integration by finite differences [15]. Although this boundary condition was taken for convenience, the

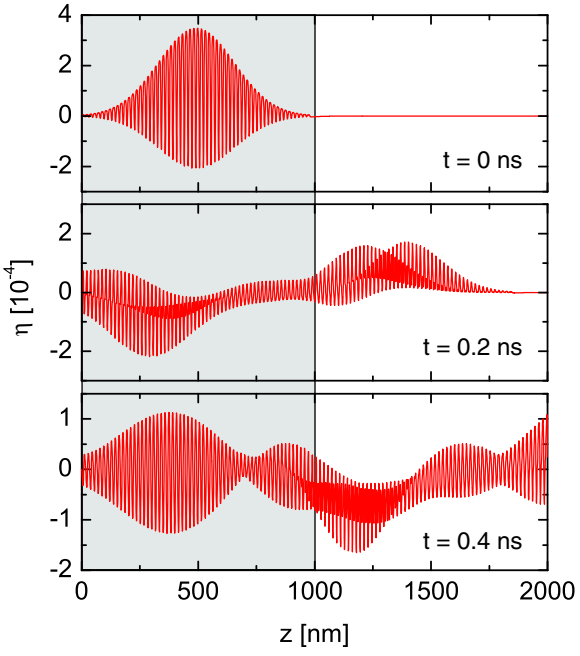

FIG. 3 (color online). Calculations of the strain propagation from the SL. The strain at $t = 0$ is a Gaussian pulse at the center of the SL (represented by the shaded area) modulated by a high-frequency component with the period of the SL. At $t = 0.2$ ns the right-propagating component reaches the substrate while the left going wave reflects from the air-SL surface. Later, at $t = 0.4$ ns, the strain propagates in the substrate as a bulk component.

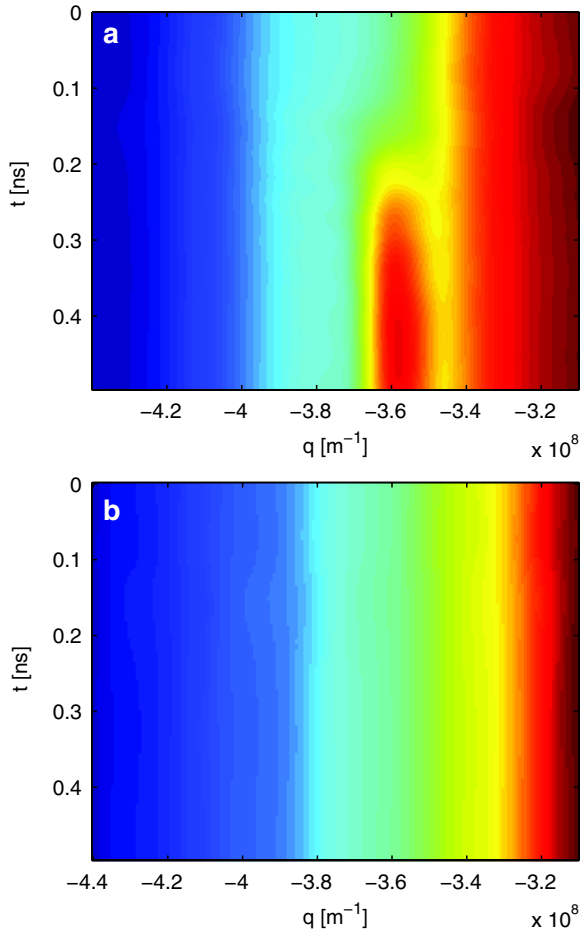

FIG. 4 (color online). Calculations of the time dependence of the diffraction due to acoustic strain below the (-1) sideband. The curves have been filtered to reproduce the experimental resolution. (a) Diffraction of the strain shown in Fig. 3. (b) Diffraction by the low frequency component of the strain.

qualitative conclusions are independent of both the boundary conditions and the specific details of the initial conditions.

Figure 3 shows the calculated time dependence of the strain. The strain associated with the folded phonons is seen as the modulation of the initial gaussian envelope with the period of the SL. The pulse is initially contained within the SL (shaded area) and results in two counterpropagating waves. At 0.2 ns the right-moving component reaches the substrate located at $z > 1000$ nm while the left-moving part reflects at the air-SL surface. After 0.4 ns, the propagating components have both reached the substrate.

In Fig. 4(a) we show the calculated time-dependent diffraction for the strain shown in Fig. 3. The results have been artificially broadened to account for the experimental peak widths and the temporal resolution. The wave vector $q = -3.6 \times 10^8$ m^{-1} agrees with the unfolded phonon position relative to the InP. The signal at this wave vector appears delayed by the transit time through the SL, $\sim$0.2 ns, as we observe in the experiment. Calculations over a finer range reveal that this signature oscillates with the period of the phonon. In addition, the strain inside the SL modulates the SL sideband with the period of the folded phonon, as previously reported [5,6]. In contrast with (a), the results shown in (b) correspond to what would occur if only the low-frequency component in the lowest acoustic branch were excited, that is, in the absence of the zone-folding and the subsequent unfolding. In this case there is no time-dependent signal at the SL wave vector. Therefore, these calculations support the attribution of coherent high-wave-vector unfolded phonon detected in the InP substrate.

In conclusion, we used time-resolved x-ray diffraction to probe the unfolding of the coherent longitudinal acoustic phonons from a SL into large-wave-vector bulk modes of the InP substrate. The observed excitation appears with a wave vector 3.6×10^8 m^{-1}, which corresponds to $\sim$7% of the Brillouin zone edge of bulk InP. While our experiment concentrated on longitudinal modes, we note that if transverse modes are excited [16] the unfolding could be observed as sidebands to an asymmetric Bragg reflection. Coherent lattice excitations of such high wave vector are inaccessible to ordinary light scattering techniques due to the long wavelength (small wave vector) of optical radiation. Our results show that such excitations can be probed with x-ray diffraction and opens the possibility to study the mean free path and transport across interfaces of short-wavelength lattice excitations that are important to thermal transport at the nanoscale. Moreover, the sensitivity to high-wave-vector acoustic waves shows the potential of TRXD to follow the dynamics of an optically excited solid at any wave vector, and could be used to measure, in time domain, the nonequilibrium phonon population throughout the whole Brillouin zone of the crystal [17].

This work was conducted at the sector 7 insertion device beam line at the APS and was supported in part by the U.S. DOE, Grants No. DE-FG02-00ER1503, the NSF FOCUS Physics Frontier Center, Grant No. PHY-0114336, the NSF Focused Research Group, Grant No. 0606406, and the Air Force Office of Scientific Research under Contract FA9550-08-1-0340 through the Multidisciplinary University Research Initiative Program. M. T. and D. A. R. thank D. Walko for experimental assistance. Use of the Advanced Photon Source was supported by the U. S. Department of Energy, Office of Science, Office of Basic Energy Sciences, under Contract No. DE-AC02-06CH11357.

*mtrigo@umich.edu
†Present address: Department of Physics, DePaul University, Chicago, IL, USA.

[1] D. G. Cahill, W. K. Ford, K. E. Goodson, G. D. Mahan, A. Majumdar, H. J. Maris, R. Merlin, and S. R. Phillpot, J. Appl. Phys. **93**, 793 (2003).
[2] B. C. Daly, N. C. R. Holme, T. Buma, C. Branciard, and T. B. Norris, Appl. Phys. Lett. **84**, 5180 (2004).
[3] R. Merlin, Solid State Commun. **102**, 207 (1997).
[4] D. A. Reis and A. M. Lindenberg, in *Light Scattering in Solids IX*, edited by M. Cardona and R. Merlin (Springer-Verlag, Berlin, 2007), p. 371.
[5] M. Bargheer, N. Zhavoronkov, Y. Gritsai, J. C. Woo, D. S. Kim, M. Woerner, and T. Elsaesser, Science **306**, 1771 (2004).
[6] P. Sondhauss, J. Larsson, M. Harbst, G. A. Naylor, A. Plech, K. Scheidt, O. Synnergren, M. Wulff, and J. S. Wark, Phys. Rev. Lett. **94**, 125509 (2005).
[7] D. A. Reis, M. F. DeCamp, P. H. Bucksbaum, R. Clarke, E. Dufresne, M. Hertlein, R. Merlin, R. Falcone, H. Kapteyn, M. M. Murnane *et al.*, Phys. Rev. Lett. **86**, 3072 (2001).
[8] S. H. Lee, A. L. Cavalieri, D. M. Fritz, M. C. Swan, R. S. Hegde, M. Reason, R. S. Goldman, and D. A. Reis, Phys. Rev. Lett. **95**, 246104 (2005).
[9] S. M. Rytov, Akust. Zh. **2**, 71 (1956)] [Sov. Phys. Acoust. **2**, 68 (1956)].
[10] M. Trigo, T. A. Eckhause, J. K. Wahlstrand, R. Merlin, M. Reason, and R. S. Goldman, Appl. Phys. Lett. **91**, 023115 (2007).
[11] S. Takagi, Acta Crystallogr. **15**, 1311 (1962).
[12] D. Taupin, Bull. Soc. Fr. Mineral. Cristallogr. **87**, 469 (1964).
[13] B. W. Batterman and H. Cole, Rev. Mod. Phys. **36**, 681 (1964).
[14] C. R. Wie and H. M. Kim, J. Appl. Phys. **69**, 6406 (1991).
[15] S. A. Teukolsky, W. T. Vetterling, and B. P. Flannery, *Numerical Recipes in C* (Cambridge University Press, Cambridge, England, 2002).
[16] C. Rossignol, J. M. Rampnoux, M. Perton, B. Audoin, and S. Dilhaire, Phys. Rev. Lett. **94**, 166106 (2005).
[17] D. B. McWhan, P. Hu, M. A. Chin, and V. Narayanamurti, Phys. Rev. B **26**, 4774 (1982).